Contribution from the School of Chemical Sciences, University of Illinois, Urbana, Illinois 61801, and Department of Chemistry, University of Virginia, Charlottesville, Virginia 22901

Dynamics of Spin-State Interconversion and Cooperativity for Ferric Spin-Crossover Complexes in the Solid State. 3.[1] Bis[*N*-(2-(benzylamino)ethyl)salicylaldiminato]iron(III) Complexes

MARK D. TIMKEN,[2] DAVID N. HENDRICKSON,*[2] and EKKEHARD SINN*[3]

Received January 31, 1985

The spin-crossover phenomenon is examined for a number of complexes with the composition $[Fe(X\text{-}SalBzen)_2]Y$, where X-SalBzen is the N_3O ligand derived from the Schiff-base condensation of *N*-benzylethylenediamine and X-substituted salicylaldehyde and Y is Cl^-, NO_3^-, or BPh_4^-. The single-crystal X-ray structure of $[Fe(3\text{-allyl-}SalBzen)_2]NO_3$ has been determined at room temperature by using heavy-atom, least-squares methods, in conjunction with data measured on a four-circle diffractometer, to give $R = 0.097$ and $R_w = 0.109$ for 4810 observed ($F_o^2 > 3\sigma(F_o^2)$) reflections. The compound crystallizes in the monoclinic space group $P2_1/c$ with four formula weights in a cell having the dimensions $a = 17.887$ (4) Å, $b = 21.686$ (6) Å, $c = 21.436$ (11) Å, and $\beta = 99.71$ (5)°. Two crystallographically independent $[Fe(3\text{-allyl-}SalBzen)_2]^+$ cations are present. The same meridional configuration of two N_3O tridentate ligands is found for both of the cations, where the oxygen atoms on the two N_3O ligands are located cis relative to each other and the imino nitrogen atoms are trans. The metal–ligand atom distances in the two different cations are different and indicate that one cation is a low-spin iron(III) complex and the other iron(III) cation is intermediate between low and high spin (i.e., a spin-crossover complex). The difference in the *average* metal–ligand bond lengths between the two different cations is 0.046 Å. Variable-temperature Mössbauer, EPR, and magnetic susceptibility results are in agreement with the view that $[Fe(3\text{-allyl-}SalBzen)_2]NO_3$ consists of equal amounts of low-spin cations and cations that are spin crossover with a description of 67% low-spin and 33% high-spin at room temperature. $[Fe(3\text{-OEt-}SalBzen)_2]BPh_4\cdot CH_3CN$ was found to undergo a spin-crossover transformation that is gradual and relatively complete with a high-spin mole fraction of 0.93 at 300 K, decreasing to 0.03 at 10 K. Slow paramagnetic relaxation for both the high- and low-spin states of $[Fe(3\text{-OEt-}SalBzen)_2]BPh_4\cdot CH_3CN$ results in sharp, well-resolved EPR signals, but extremely broad Mössbauer absorptions. Even with a 43% ^{57}Fe-enriched sample of this compound, the signals in the Mössbauer spectrum are too broad to tell if separate high- and low-spin signals are present at temperatures above 190 K.

Introduction

For a variety of first-row transition-metal complexes the near-equivalence of the ligand field splitting energy and the spin-pairing energy gives rise to high- and low-spin electronic states that lie within thermal energy of each other.[4] These co-called spin-crossover complexes exhibit temperature-dependent changes in the relative populations of the high- and low-spin electronic states. A number of recent research efforts in the area of spin-crossover chemistry have focused on understanding the thermal high-spin–low-spin transformation in the *solid* state. These efforts have included attempts to better characterize the factors that affect the bulk nature of the spin-crossover transformation (i.e., thermally discontinuous vs. gradual transformations), as well as attempts to identify factors that affect the rates of intramolecular spin-state interconversion.

In the former category, König and co-workers[5] have used variable-temperature X-ray powder methods to characterize transformations of the discontinuous and gradual types. Discontinuous transformations show evidence for distinct high- and low-spin lattices; that is, the spin-crossover transformation is accompanied by a structural transition. In fact, it has been suggested repeatedly that discontinuous transformations are essentially first-order phase transitions, where high- and low-spin domains are present and cooperative intermolecular interactions play an important role. Gradual transformations, on the other hand, show evidence for a *single* lattice with unit cell parameters that change continuously with temperature. Apparently, the high- and low-spin molecules are situated randomly within a lattice that can accommodate both species.

The factors that influence the intramolecular spin-state lifetime τ

$$\tau = 1/(k_1 + k_{-1})$$

for

$$\text{low spin} \underset{k_{-1}}{\overset{k_1}{\rightleftharpoons}} \text{high spin}$$

in spin-crossover complexes are less well-defined. Solution interconversion lifetimes have been determined for a variety of Co^{II}, Fe^{II}, and Fe^{III} spin-crossover systems by laser Raman *T*-jump[6] and ultrasonic[7] kinetics methods. These lifetimes (at room temperature) fall in the range of 80–<30 ns for Co^{II} complexes, 120–30 ns for Fe^{II} complexes, and 60–<1 ns for Fe^{III} complexes. The fastest rates occur for the ferric dithiocarbamates, for which the lifetimes are too short to determine accurately. Several experiments have led to suggestions that intramolecular steric interactions play a significant role in controlling the spin-state interconversion rates.

The characterization of spin-state interconversion rates for spin-crossover *solids* relies on the use of the time scales associated with various spectroscopic techniques. Such determinations typically result only in a bracketing of the rate. These investigations, however, can potentially provide insight into the effects of intermolecular interactions on the spin-state interconversion rates. For ferric spin-crossover systems, Mössbauer and EPR spectroscopy, with inverse time scales of $\sim 10^7$ s^{-1} and $\sim 10^{10}$ s^{-1}, respectively, have been important tools. The ferric dithio-

(1) Part 1: Federer, W. D.; Hendrickson, D. N. *Inorg. Chem.* **1984**, *23*, 3861. Part 2: Federer, W. D.; Hendrickson, D. N. *Inorg. Chem.* **1984**, *23*, 3870.
(2) University of Illinois.
(3) University of Virginia.
(4) For reviews see: (a) Barefield, E. K.; Busch, D. H.; Nelson, S. M. *Q. Rev., Chem. Soc.* **1968**, *22*, 457. (b) Martin, R. L.; White, A. H. *Transition Met. Chem. (N.Y.)* **1968**, *4*, 113. (c) Gütlich, P. *Struct. Bonding (Berlin)* **1981**, *44*, 83.
(5) (a) König, E.; Ritter, G.; Irler, W.; Goodwin, H. A. *J. Am. Chem. Soc.* **1980**, *102*, 4681. (b) König, E.; Ritter, G.; Kulsbreshtha, S. K.; Nelson, S. M. *J. Am. Chem. Soc.* **1983**, *105*, 1924.
(6) (a) Beattie, J. K.; Sutin, N.; Turner, D. H.; Flynn, G. W. *J. Am. Chem. Soc.* **1973**, *95*, 2052. (b) Hoselton, M. A.; Drago, R. S.; Wilson, L. J. *J. Am. Chem. Soc.* **1976**, *98*, 6967. (c) Tweedle, M. F.; Wilson, L. J. *J. Am. Chem. Soc.* **1976**, *98*, 4824; (d) Dose, E. V.; Murphy, K. M. M.; Wilson, L. J. *Inorg. Chem.* **1976**, *15*, 2622. (e) Simmons, M. G.; Wilson, L. J. *Inorg. Chem.* **1977**, *16*, 126. (f) Dose, E. V.; Hoselton, M. A.; Sutin, N.; Tweedle, M. F.; Wilson, L. J. *J. Am. Chem. Soc.* **1978**, *100*, 1141.
(7) (a) Beattie, J. K.; Binstead, R. A.; West, R. J. *J. Am. Chem. Soc.* **1978**, *100*, 3044. (b) Binstead, R. A.; Beattie, J. K.; Dose, E. V.; Tweedle, M. F.; Wilson, L. J. *J. Am. Chem. Soc.* **1978**, *100*, 5609. (c) Binstead, R. A.; Beattie, J. K.; Dewey, T. G.; Turner, D. H. *J. Am. Chem. Soc.* **1980**, *102*, 6442.

0020-1669/85/1324-3947$01.50/0

carbamates,[8] monothiocarbamates,[9] and diselenocarbamates[10] were, until recently, the only ferric complexes known to interconvert rapidly on the Mössbauer time scale. Furthermore, the dithiocarbamates were shown[11] to exhibit complicated but essentially distinct high- and low-spin EPR signals, from which it was inferred that 0.1 ns $\leq \tau \leq$ 100 ns. Maeda et al.[12] and Federer et al.[1] have discovered a number of new ferric complexes with N_4O_2 ligand donor atoms that also undergo rapid spin-state interconversion on the Mössbauer time scale and slow interconversion on the EPR time scale. Several of the complexes are unique in that they exhibit interconversion rates that are extremely sensitive to seemingly small molecular and structural changes. For example,[12] the complex $[Fe(acen)(pic)_2]BPh_4$ where acen is *N*,*N'*-bis(1-methyl-3-oxobutylidene)ethylenediamine and pic is 4-methylpyridine, exhibits rapid spin-state interconversion on the Mössbauer time scale, whereas the very similar complex $[Fe(acen)(lut)_2]BPh_4$, where lut is 3,4-dimethylpyridine, exhibits slow spin-state interconversion. Furthermore,[12] the complex $[Fe(acpa)_2]BPh_4 \cdot H_2O$, where Hacpa is *N*-(1-acetyl-2-propylidene)-2-pyridylmethylamine, exhibits rapid Mössbauer interconversion while the corresponding monohydrated PF_6^- salt is slow on the Mössbauer time scale. The origins of these differences are not understood, although the influences of subtle intra- and intermolecular steric interactions are implicated.

Such observations motivated our interest in examining the spin-state interconversion rates in other ferric N_4O_2 spin-crossover solids. In particular, the ferric SalRen complexes[13,14] $[Fe(X\text{-}SalRen)_2]^+$ looked to be promising candidates for further study.

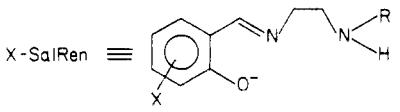

SalMeen: R = methyl
SalEen: R = ethyl
SalBzen: R = benzyl

Solution rate studies[13] on several Salmeen complexes indicated spin-state interconversion rates of ca. 10^7–10^8 s^{-1}, although Mössbauer spectroscopy[13,14] of corresponding solids showed rates of less than 10^7 s^{-1}. These observations suggest that the spin-state lifetimes in these systems may be quite close to the Mössbauer spectroscopic time scale. With this in mind, we have prepared the new, but closely related, $[Fe(X\text{-}SalBzen)_2]^+$ complexes. In this paper we report the spectroscopic and structural characterization of several of these new complexes. These results, particularly the variable-temperature EPR data, are discussed in terms of the various solid-state spin-crossover mechanisms. Some difficulties that can be encountered when interpreting the Mössbauer spectra of ferric spin-crossover solids are also described.

Experimental Section

Compound Preparation. All reagents and solvents were commercially available and used without further purification. The ^{57}Fe powder (95% enriched) was obtained from New England Nuclear. Elemental analyses were performed in the Microanalytical Laboratory of the School of Chemical Sciences, University of Illinois.

$[Fe(3\text{-}OEt\text{-}SalBzen)_2]NO_3$. A sample was prepared by following the method of Haddad et al.[14] The Schiff-base ligand was formed by adding a solution of 1.5 g (10 mmol) of *N*-benzylethylenediamine in 15 mL of methanol to a solution of 1.66 g (10 mmol) of 3-ethoxysalicylaldehyde in 15 mL of methanol. As the yellow Schiff-base solution was stirred, 0.4 g NaOH in 5 mL of methanol was added, followed by the dropwise addition of 2 g (5 mmol) of $Fe(NO_3)_3 \cdot 9H_2O$ in 15 mL of methanol. Addition of the ferric solution led to the immediate precipitation of black microcrystals, which were isolated by filtration, washed with methanol and ether, and then dried in vacuo to give 3.3 g (89% yield) of product. Anal. Calcd for $FeC_{36}H_{42}N_5O_7$: C, 60.69; H, 5.62; N, 9.83; Fe, 7.85. Found: C, 60.31; H, 5.86; N, 9.73; Fe, 7.52.

$[Fe(3\text{-}OEt\text{-}SalBzen)_2]Cl$. The procedure used to prepare this compound is identical with that for $[Fe(3\text{-}OEt\text{-}SalBzen)_2]NO_3$ except that 0.81 g of $FeCl_3$ was used instead of $Fe(NO_3)_3 \cdot 9H_2O$. Additionally, it was necessary to refrigerate the reaction mixture for 1 day following the addition of the ferric solution in order to promote precipitation of the dark purple microcrystalline product. The product was isolated and washed as above to give a yield of 3.1 g (91%). Anal. Calcd for $FeC_{36}O_4N_4H_{42}Cl$: C, 63.28; H, 5.91; N, 8.20; Fe, 8.17. Found: C, 62.76; H, 6.23; N, 8.22; Fe, 8.29.

$[Fe(3\text{-}All\text{-}SalBzen)_2]NO_3$ (All = Allyl). The reagent quantities were identical with those used for $[Fe(3\text{-}OEt\text{-}SalBzen)_2]NO_3$, except that 1.62 g of 3-allylsalicylaldehyde was used in place of 3-ethoxysalicylaldehyde. After the reactants were combined as above, overnight refrigeration of the reaction mixture afforded only a small amount of dark powder, which was isolated by filtration and washed with methanol and ether. The filtrate was allowed to stand for 1 week and yielded a number of large blue-purple plates, which were isolated and saved for single-crystal X-ray diffraction studies. The filtrate also afforded 0.7 g (20% yield) of blue-purple microcrystals, which were isolated by filtration, washed with water, air dried, and then vacuum dried. Anal. Calcd for $FeC_{38}H_{42}N_5O_5$: C, 64.78; H, 5.97; N, 9.94; Fe, 7.93. Found: C, 63.94; H, 5.79; N, 10.02; Fe, 7.83.

$[Fe(3\text{-}OEt\text{-}SalBzen)_2]BPh_4$. This compound was isolated in several ways due to the necessity of preparing it from 95%-enriched ^{57}Fe powder for Mössbauer work. The different preparations are described below.

(a) Unenriched $[Fe(3\text{-}OEt\text{-}SalBzen)_2]BPh_4$ was prepared by metathesis (twofold molar excess of $NaBPh_4$) of the corresponding nitrate salt in hot methanol. Anal. Calcd for $FeC_{60}H_{62}N_4O_4B$: C, 74.45; H, 6.20; N, 5.79; Fe, 5.78. Found: C, 73.98; H, 6.56, N, 5.76; Fe, 5.75.

(b) ^{57}Fe-enriched $[Fe(3\text{-}OEt\text{-}SalBzen)_2]BPh_4$ was prepared by first dissolving 25 mg (0.45 mmol) of ^{57}Fe powder in 8 mL of concentrated hydrochloric acid; dissolution was accelerated by stirring and heating at 50 °C for 5 min. The resulting yellow-orange solution was evaporated under reduced pressure to give a yellow-orange powder, which was then dissolved in 5 mL of methanol. A solution of the Schiff-base ligand was prepared by combining 0.15 g (1 mmol) of *N*-benzylethylenediamine and 0.17 g (1 mmol) of 3-ethoxybenzaldehyde in 10 mL of methanol. The methanolic iron chloride solution was then added dropwise to the ligand solution with heat and stirring, at which time the reaction mixture immediately turned dark purple. Following the dropwise addition of 0.68 g (2 mmol) of $NaBPh_4$ in 5 mL of methanol to the reaction mixture, black-purple microcrystals formed within a few minutes. The product was isolated by filtration, washed with ether, and air dried to give 0.29 g (61% yield) of product.

(c) ^{57}Fe-enriched $[Fe(3)\text{-}OEt\text{-}SalBzen)_2]BPh_4 \cdot CH_3CN$ was prepared by recrystallization of the BPh_4^- salt in acetonitrile. In order to facilitate sample handling, 0.14 g of the 95% enriched compound prepared in (b) was combined with 0.18 g of the unenriched (2.1% ^{57}Fe) material prepared in (a) to give a sample enriched to 43%. All 0.32 g was dissolved in 10 mL of boiling acetonitrile. After the total volume was slowly boiled down to ca. 5 mL, the solution was refrigerated overnight to obtain a purple-black microcrystalline product. The material was isolated by filtration, washed with ether, and air dried to give 0.265 g (80% yield). This material, which was analyzed for one acetonitrile solvate per complex ion, was divided into three portions for further study.

I. This portion was comprised of 99.9 mg of the unperturbed, microcrystalline complex $[Fe(3\text{-}OEt\text{-}SalBzen)_2]BPh_4 \cdot CH_3CN$. Anal. Calcd for $FeC_{62}H_{65}N_5O_4B$: C, 73.65; H, 6.49; N, 6.93. Found: C 72.91; H, 6.61; N, 7.53.

II. For this portion, 85.7 mg of I was lightly ground in a ceramic mortar and pestle for 2 min. Anal. Calcd for $FeC_{62}H_{65}N_5O_4B$: C, 73.65; H, 6.49; N, 6.93. Found: C, 73.35; H, 6.57; N, 7.13.

III. A 79.4-mg sample of I was heated at 65 °C in vacuo for 10 h. The experimental weight loss of 3.3 mg was in excellent agreement with the 3.2-mg loss expected for desolvation of one CH_3CN per formula unit. Elemental analysis concurs with the formulation $[Fe(3\text{-}OEt\text{-}SalBzen)_2]BPh_4$. Anal. Calcd for $FeC_{60}H_{62}N_4O_4B$: C, 74.45; H, 6.20; N, 5.79. Found: C, 72.67; H, 6.40; N, 6.04.

(8) Merrithew, P. B.; Rasmussen, P. G. *Inorg. Chem.* **1972**, *11*, 325.
(9) Kunze, K. R.; Perry, D. L.; Wilson, L. J. *Inorg. Chem.* **1977**, *16*, 594.
(10) DeFilipo, D.; Depalano, P.; Diaz, A.; Steffe, S.; Trogu, E. F. *J. Chem. Soc., Dalton Trans.* **1977**, 1566.
(11) Hall, G. R.; Hendrickson, D. N. *Inorg. Chem.* **1976**, *15*, 607.
(12) (a) Maeda, Y.; Tsutsumi, N.; Takashima, Y. *Chem. Phys. Lett.* **1982**, *88*, 248. (b) Maeda, Y.; Ohshio, H.; Takashima, Y. *Chem. Lett.* **1982**, 943. (c) Ohshio, H.; Maeda, Y.; Takashima, Y. *Inorg. Chem.* **1983**, *22*, 2684. (d) Maeda, Y.; Tsutsumi, N.; Takashima, Y. *Inorg. Chem.* **1984**, *23*, 2440.
(13) Petty, R. H.; Dose, E. V.; Tweedle, M. F.; Wilson, L. J. *Inorg. Chem.* **1978**, *17*, 1064.
(14) (a) Haddad, M. S.; Federer, W. D.; Lynch, M. W.; Hendrickson, D. N. *J. Am. Chem. Soc.* **1980**, *102*, 1468. (b) Haddad, M. S.; Lynch, M. W.; Federer, W. D.; Hendrickson, D. N. *Inorg. Chem.* **1981**, *20*, 123. (c) Haddad, M. S.; Federer, W. D.; Lynch, M. W.; Hendrickson, D. N. *Inorg. Chem.* **1981**, *20*, 131.

Table I. Crystal Data for $[Fe(3\text{-All-SalBzen})_2]NO_3$

formula: $Fe_2O_{10}N_{10}C_{76}H_{84}$ (two monomolecular units)	mol wt = 1409
space group: $P2_1/c$	$Z = 4$
$a = 17.887$ (4) Å	$\alpha = 90°$
$b = 21.686$ (6) Å	$\beta = 99.71$ (5)°
$c = 21.436$ (11) Å	$\gamma = 90°$
$V = 8196$ Å^3	μ(MoKα) = 4.2 cm^{-1}
$\rho_{calcd} = 1.14$ g cm^{-3}	$\rho_{obsd} = 1.19$ g cm^{-3}

We are unable to obtain single crystals of $[Fe(3\text{-OEt-SalBzen})_2]BPh_4$ in its solvated or desolvated forms that were suitable for an X-ray structural analysis.

Physical Measurements. Variable-temperature magnetic susceptibility data were obtained on two different instruments. For the unenriched (^{57}Fe) samples, a PAR Model 150A vibrating-sample magnetometer, operated at 13.5 kG, was used to collect data on microcrystalline samples. The magnetometer was calibrated with $CuSO_4 \cdot 5H_2O$, and a calibrated GaAs diode was used for sample temperature determination and control. For the ^{57}Fe-enriched samples, data were collected on a Series 800 VTS-50 SQUID susceptometer (SHE Corp.). A magnetic field of 10 kG was used. For all data, diamagnetic corrections, estimated from Pascal's constants, were used in the calculation of molar paramagnetic susceptibilities.

Electron paramagnetic resonance data (X-band) were collected with the use of a Varian E-9 spectrometer. The magnetic field was calibrated with a Bruker B-NM 20 NMR oscillator; a DPPH marker gauged the microwave frequency. Variable temperatures (300–130 K) were obtained with the use of a gas-flow cavity insert and a Varian V-4540 temperature controller. Temperatures were determined before and after each spectrum with a Cu–constantan thermocouple; temperature precision is estimated to be ±5 K. A direct-immersion Dewar, which was inserted into the cavity, was used to obtain 77 K data. Spectra at Q-band frequencies were run on a Varian E-15 spectrometer operating at 35 GHz.

Mössbauer (^{57}Fe) data were collected on a previously described instrument.[15] Sample temperatures were controlled by a Lake Shore Cryotronics Model DRC 80C temperature controller in conjunction with a Si diode mounted on the copper sample-cell holder. A Cu–constantan thermocouple and a Yellow Springs Instrument 44003A precision thermistor, both mounted on the sample-cell holder, were used to monitor the sample temperature. The absolute precision is estimated to be ±3 K; the relative precision is ±0.5 K. A previously described computer program[16] was used to fit the Mössbauer absorptions to Lorentzian line shapes. The isomer shifts reported are relative to iron foil at 298 K but are not corrected for the temperature-dependent second-order Doppler shift. Also, note that the isomer shifts shown in the figures are shifted slightly; actual isomer shift data can be found in the tabulated results.

X-ray powder diffraction patterns were obtained with the use of a Norelco (Phillips Electronics Co.) powder diffractometer equipped with a copper X-ray tube and monochromator.

Collection and Reduction of X-ray Data. The X-ray crystal data for $[Fe(3\text{-All-SalBzen})_2]NO_3$ are summarized in Table I. The crystal did not diffract strongly, a fact reflected by the limited size of the diffraction data set (vide infra). Cell dimensions and space group data were obtained by standard methods on an Enraf-Nonius four-circle CAD-4 diffractometer. The θ–2θ scan technique was used, as previously described,[17] to record the intensities for all nonequivalent reflections for which $1° < 2\theta < 49°$. Scan widths were calculated as $(A + B(\tan\theta))$, where A is estimated from the mosaicity of the crystal and B allows for the increase in peak width due to $K\alpha_1$–$K\alpha_2$ splitting. The values of A and B were 0.6 and 0.35°, respectively.

The intensities of three standard reflections showed no greater fluctuations during the data collection than those expected from Poisson statistics. The raw intensity data were corrected for Lorentz–polarization effects, but not for absorption. Of the 7625 independent intensities, there were 4810 with $F_o^2 > 3\sigma(F_o^2)$, where $\sigma(F_o^2)$ was estimated from counting statistics.[18] These data were used in the final refinement of the structural parameters.

Structure Determination. A three-dimensional Patterson synthesis was used to determine heavy-atom positions, which phased the data sufficiently well to permit location of the remaining non-hydrogen atoms from Fourier syntheses. Full-matrix least-squares refinement was carried out as previously described.[17] Anisotropic temperature factors were introduced for the heaviest atoms only, due to the limited size of the data set. Further Fourier difference functions permitted location of the non-methyl hydrogen atoms, which were included in the refinement for four cycles of least-squares refinement and then held fixed.

The model converged with $R = 0.097$ and $R_w = 0.109$. A final Fourier difference map was featureless. A listing of the observed and calculated structure factors is available together with calculated thermal parameters.[19] The principal programs used are as previously described.[17]

Results and Discussion

Molecular and Crystal Structure of $[Fe(3\text{-All-SalBzen})_2]NO_3$. Final positional parameters for the atoms are given in Table II. Table III contains the most important bond lengths and bond angles. As indicated in Tables II and III, the unit cell contains two crystallographically independent complexes. Figure 1 shows a stereoview of one of the two independent cations, while Figure 2 shows the ionic packing in the unit cell.

It is evident from Figure 1 that the two tridentate ligands provide each ferric center a pseudooctahedral coordination geometry. For both of the crystallographically independent cations the two N_2O ligands lie in nearly orthogonal planes about the metal ion. The oxygen atoms on the two ligands are located cis relative to each other; the imino nitrogen atoms are trans. This meridional geometry is, not surprisingly, identical with that found[20] for the closely related complexes $[Fe(X\text{-Salmeen})_2]PF_6$.

Although the two crystallographically independent cations possess the same gross structural features, there are significant differences in detail that are of great importance in interpreting the magnetic susceptibility data for this compound. The metal–ligand bonds in cation 1 are consistently longer than the corresponding bond distances in cation 2. The difference in the average metal–ligand bond lengths $\langle Fe\text{–}L\rangle$ is 0.046 Å. It has previously been found[20] that the difference between $\langle Fe\text{–}L\rangle_{HS}$ and $\langle Fe\text{–}L\rangle_{LS}$ lies in the range of 0.12–0.15 Å for ferric spin-crossover complexes. The 0.046-Å difference seen here corresponds to about one-third the difference between the pure high- and low-spin forms, in reasonable agreement with the magnetic and spectroscopic characterization of the corresponding microcrystalline solid (vide infra). The difference between the two cations appears quite clearly to be real; the greatest difference between the two sets of Fe–ligand bonds (0.074 Å) is between the loosest and most compressible Fe–amine bonds, while the smallest difference (0.023 Å) is between the tight, relatively incompressible Fe–O bonds. This is precisely what occurs for related FeN_4O_2 spin-crossover complexes when the proportion of high- and low-spin species is altered.

Spin-crossover transitions are known to be extremely sensitive to a number of solid-state features including the nature of the counterion,[14] the presence (or absence) of molecules of solvation,[4] and the defect structure of the solid.[14] The structure reported here highlights how a small difference in crystal packing can have a considerable effect on the spin-state fraction. All other parameters are held the same for the two cations: same ligand, same counterion, identical chemical composition in the same crystal.

Similar crystal packing effects have been seen for only a few other spin-crossover systems. For example, the room-temperature structure of a spin-crossover ferric tris(dithiocarbamate) recently reported by Terzis et al.[21] also shows two independent molecular units with different Fe–L distances ($\langle Fe_1\text{—}L\rangle = 2.406$ Å, $\langle Fe_2\text{–}L\rangle = 2.354$ Å). No spectroscopic distinction of the two sites was reported. Related observations have been described by Ryabova et al.[22] for two ferric thiosemicarbazonate complexes. These

(15) (a) Cohn, M. J.; Timken, M. D.; Hendrickson, D. N. *J. Am. Chem. Soc.* **1984**, *106*, 6683. (b) Federer, W. D. Ph.D. Thesis, University of Illinois, 1984.
(16) Chrisman, B. L.; Tumolillo, T. A. *Comput. Phys. Commun.* **1971**, *2*, 322.
(17) Freyberg, D. P.; Mockler, G. M.; Sinn, E. *J. Chem. Soc., Dalton Trans.* **1976**, 447.
(18) Corfield, P. W. R.; Doedens, R. J.; Ibers, J. A. *Inorg. Chem.* **1967**, *6*, 197.
(19) Supplementary material.
(20) Sim, G.; Sinn, E.; Petty, R. H.; Merrill, C. L.; Wilson, L. J. *Inorg. Chem.* **1981**, *20*, 213.
(21) Terzis, A.; Fillippakis, S.; Mentzafos, D.; Petrovleas, V.; Malliaris, A. *Inorg. Chem.* **1984**, *23*, 334.
(22) (a) Ryabova, N. A.; Ponomarev, V. I.; Zelentsov, V. V.; Atovmyan, L. O. *Sov. Phys.—Crystallogr. (Engl. Trans.)* **1982**, *27*, 46. (b) Ryabova, N. A.; Ponomarev, V. V.; Atovmyan, L. O. *Sov. Phys.—Crystallogr. (Engl. Trans.)* **1982**, *27*, 171.

Table II. Atomic Parameters for $[Fe(3\text{-All-SalBzen})_2]NO_3$[a]

atom	x/a	y/b	z/c	atom	x/a	y/b	z/c
Fe(1)	0.5190 (2)	0.2185 (2)	0.3930 (1)	C(13C)	0.075 (1)	1.0801 (13)	0.0410 (12)
Fe(2)	0.0412 (1)	0.8293 (1)	0.2016 (1)	C(14C)	0.144 (1)	1.0838 (13)	0.0352 (12)
O(A)	0.4148 (7)	0.2081 (7)	0.3510 (6)	C(15C)	0.196 (2)	1.0450 (14)	0.0517 (13)
O(B)	0.4980 (8)	0.2865 (8)	0.4394 (7)	C(16C)	0.167 (1)	0.9852 (13)	0.0754 (12)
O(C)	0.0092 (6)	0.7559 (6)	0.2339 (5)	C(17C)	−0.049 (1)	0.6422 (13)	0.2476 (12)
O(D)	−0.0585 (7)	0.8554 (6)	0.1661 (6)	C(18C)	0.028 (2)	0.6075 (15)	0.2610 (15)
O(1)	0.7446 (10)	0.1125 (9)	−0.1828 (8)	C(19C)	0.066 (2)	0.5971 (19)	0.2125 (19)
O(2)	0.7514 (12)	0.0565 (10)	−0.2636 (10)	C(1D)	−0.085 (1)	0.7774 (9)	0.0868 (8)
O(3)	0.6479 (12)	0.0634 (11)	−0.2354 (11)	C(2D)	−0.104 (1)	0.8241 (10)	0.1252 (9)
O(4)	0.7410 (13)	0.1399 (12)	0.3676 (11)	C(3D)	−0.186 (1)	0.8451 (11)	0.1205 (11)
O(5)	0.8106 (22)	0.0789 (20)	0.4093 (19)	C(4D)	−0.233 (1)	0.8081 (11)	0.0761 (11)
O(6)	0.7050 (16)	0.0846 (14)	0.4245 (13)	C(5D)	−0.215 (1)	0.7646 (11)	0.0409 (10)
N(1A)	0.5393 (8)	0.2704 (8)	0.3220 (7)	C(6D)	−0.141 (1)	0.7475 (11)	0.0443 (10)
N(2A)	0.6380 (9)	0.2348 (8)	0.4237 (7)	C(7D)	−0.005 (1)	0.7592 (9)	0.0877 (9)
N(1B)	0.4986 (9)	0.1620 (8)	0.4613 (7)	C(8D)	0.127 (1)	0.7627 (9)	0.1242 (9)
N(2B)	0.5437 (10)	0.1333 (9)	0.3553 (8)	C(9D)	0.161 (1)	0.7455 (9)	0.1916 (9)
N(1C)	0.0301 (8)	0.8781 (7)	0.2759 (7)	C(10D)	0.171 (1)	0.7829 (10)	0.3025 (9)
N(2C)	0.0800 (9)	0.9102 (8)	0.1717 (7)	C(11D)	0.252 (1)	0.7566 (9)	0.3203 (8)
N(1D)	0.0515 (8)	0.7823 (7)	0.1273 (7)	C(12D)	0.309 (1)	0.7976 (10)	0.3346 (10)
N(2D)	0.1512 (8)	0.8000 (7)	0.2309 (6)	C(13D)	0.385 (1)	0.7730 (11)	0.3518 (10)
N(1)	0.7189 (12)	0.0783 (11)	−0.2243 (10)	C(14D)	0.392 (1)	0.7116 (11)	0.3521 (10)
N(2)	0.7541 (18)	0.0968 (17)	0.3976 (15)	C(15D)	0.339 (1)	0.6705 (12)	0.3411 (11)
C(1A)	0.408 (1)	0.2862 (10)	0.2723 (9)	C(16D)	0.263 (1)	0.6943 (10)	0.3228 (10)
C(2A)	0.379 (1)	0.2454 (10)	0.3080 (9)	C(17D)	−0.207 (1)	0.8986 (12)	0.1540 (11)
C(3A)	0.295 (1)	0.2319 (11)	0.2961 (10)	C(18D)	−0.188 (2)	0.9620 (16)	0.1329 (16)
C(4A)	0.260 (1)	0.2720 (11)	0.2514 (11)	C(19D)	−0.217 (3)	0.9942 (28)	0.1237 (26)
C(5A)	0.284 (1)	0.3137 (12)	0.2154 (11)	C(18B′)	0.550 (3)	0.4276 (26)	0.5248 (25)
C(6A)	0.363 (1)	0.3206 (11)	0.2246 (11)	H(4A)	0.205 (8)	0.264 (7)	0.250 (7)
C(7A)	0.491 (1)	0.2984 (10)	0.2795 (9)	H(5A)	0.251 (8)	0.340 (7)	0.183 (7)
C(8A)	0.622 (1)	0.2836 (11)	0.3201 (10)	H(6A)	0.387 (8)	0.351 (7)	0.201 (6)
C(9A)	0.655 (1)	0.2911 (11)	0.3927 (10)	H(7A)	0.508 (8)	0.332 (7)	0.251 (7)
C(10A)	0.658 (1)	0.2462 (12)	0.4942 (11)	H(81A)	0.642 (8)	0.252 (7)	0.304 (6)
C(11A)	0.750 (1)	0.2562 (10)	0.5172 (10)	H(82A)	0.628 (8)	0.325 (7)	0.294 (6)
C(12A)	0.792 (1)	0.2098 (11)	0.5246 (10)	H(91A)	0.631 (7)	0.329 (7)	0.410 (6)
C(13A)	0.875 (1)	0.2197 (11)	0.5446 (10)	H(92A)	0.706 (8)	0.297 (7)	0.396 (7)
C(14A)	0.891 (1)	0.2781 (1)	0.5500 (10)	H(N2A)	0.659 (7)	0.199 (7)	0.412 (6)
C(15A)	0.853 (1)	0.3280 (12)	0.5409 (11)	H(10A1)	0.631 (8)	0.282 (7)	0.505 (7)
C(16A)	0.770 (1)	0.3140 (11)	0.5214 (10)	H(10A2)	0.647 (8)	0.209 (7)	0.512 (6)
C(17A)	0.267 (1)	0.1795 (12)	0.3281 (12)	H(12A)	0.773 (7)	0.166 (7)	0.520 (6)
C(18A)	0.269 (2)	0.1133 (14)	0.3016 (13)	H(13A)	0.910 (8)	0.185 (7)	0.549 (6)
C(19A)	0.289 (2)	0.1014 (16)	0.2425 (15)	H(14A)	0.938 (8)	0.285 (7)	0.562 (6)
C(1B)	0.442 (1)	0.2376 (10)	0.5210 (9)	H(15A)	0.871 (8)	0.372 (7)	0.543 (6)
C(2B)	0.460 (1)	0.2888 (10)	0.4894 (9)	H(16A)	0.734 (8)	0.350 (7)	0.513 (7)
C(3B)	0.443 (1)	0.3500 (12)	0.5132 (11)	H(17A1)	0.290 (8)	0.180 (7)	0.370 (7)
C(4B)	0.403 (2)	0.3522 (13)	0.5599 (13)	H(17A2)	0.216 (8)	0.190 (7)	0.332 (7)
C(5B)	0.387 (1)	0.3045 (12)	0.5875 (12)	H(4B)	0.387 (8)	0.391 (7)	0.578 (7)
C(6B)	0.403 (1)	0.2447 (13)	0.5721 (12)	H(5B)	0.360 (8)	0.308 (7)	0.625 (6)
C(7B)	0.462 (1)	0.1776 (10)	0.5067 (9)	H(6B)	0.388 (7)	0.206 (7)	0.592 (6)
C(8B)	0.514 (1)	0.1006 (13)	0.4511 (12)	H(7B)	0.446 (8)	0.147 (7)	0.530 (6)
C(9B)	0.507 (1)	0.0845 (12)	0.3841 (11)	H(81B)	0.566 (8)	0.096 (7)	0.467 (6)
C(10B)	0.527 (1)	0.1265 (11)	0.2828 (11)	H(82B)	0.485 (8)	0.075 (7)	0.471 (7)
C(11B)	0.544 (1)	0.0715 (11)	0.2518 (10)	H(91A)	0.454 (8)	0.085 (7)	0.366 (6)
C(12B)	0.622 (2)	0.0528 (13)	0.2592 (13)	H(92B)	0.526 (8)	0.047 (7)	0.376 (7)
C(13B)	0.636 (2)	−0.0064 (15)	0.2318 (14)	H(N2B)	0.597 (8)	0.124 (7)	0.365 (7)
C(14B)	0.581 (2)	−0.0385 (14)	0.1992 (13)	H(10B1)	0.476 (8)	0.136 (7)	0.271 (7)
C(15B)	0.510 (2)	−0.0202 (15)	0.1879 (15)	H(10B2)	0.557 (8)	0.163 (7)	0.268 (7)
C(16B)	0.490 (1)	0.0344 (13)	0.2218 (12)	H(12B)	0.662 (8)	0.080 (7)	0.278 (7)
C(17B)	0.461 (2)	0.4031 (17)	0.4813 (16)	H(13B)	0.691 (8)	−0.020 (7)	0.231 (7)
C(18B)	0.505 (6)	0.4240 (53)	0.4593 (51)	H(14B)	0.601 (8)	−0.076 (7)	0.181 (7)
C(19B)	0.586 (3)	0.4354 (26)	0.4781 (26)	H(15B)	0.470 (8)	−0.044 (7)	0.159 (7)
C(1C)	−0.042 (1)	0.7995 (8)	0.3207 (8)	H(16B)	0.435 (8)	0.042 (7)	0.225 (7)
C(2C)	−0.032 (1)	0.7515 (9)	0.2817 (8)	H(4C)	−0.120 (8)	0.639 (7)	0.344 (6)
C(3C)	−0.061 (1)	0.6909 (9)	0.2891 (9)	H(5C)	−0.139 (8)	0.723 (7)	0.410 (7)
C(4C)	−0.103 (1)	0.6820 (11)	0.3378 (10)	H(6C)	−0.095 (7)	0.823 (6)	0.397 (6)
C(5C)	−0.111 (1)	0.7315 (11)	0.3754 (10)	H(7C)	−0.020 (7)	0.891 (7)	0.347 (6)
C(6C)	−0.085 (1)	0.7895 (10)	0.3708 (9)	H(81C)	0.033 (8)	0.964 (7)	0.302 (6)
C(7C)	−0.010 (1)	0.8591 (9)	0.3195 (8)	H(82C)	0.112 (8)	0.941 (7)	0.298 (6)
C(8C)	0.061 (1)	0.9392 (10)	0.2775 (10)	H(91C)	0.082 (8)	0.999 (7)	0.211 (6)
C(9C)	0.055 (1)	0.9602 (10)	0.2112 (10)	H(92C)	0.005 (8)	0.972 (7)	0.196 (6)
C(10C)	0.063 (1)	0.9239 (10)	0.1029 (10)	H(N2C)	0.133 (8)	0.911 (7)	0.176 (7)
C(11C)	0.091 (1)	0.9808 (10)	0.0820 (10)	H(10C1)	0.083 (7)	0.891 (6)	0.082 (6)
C(12C)	0.047 (1)	1.0304 (11)	0.0651 (11)	H(10C2)	0.009 (8)	0.924 (7)	0.089 (6)

[a] Atoms that are labeled with A and B are part of the two tridentate ligands of one of the two different cations (see Figure 1). The atoms labeled with C and D are part of the two tridentate ligands of the second cation.

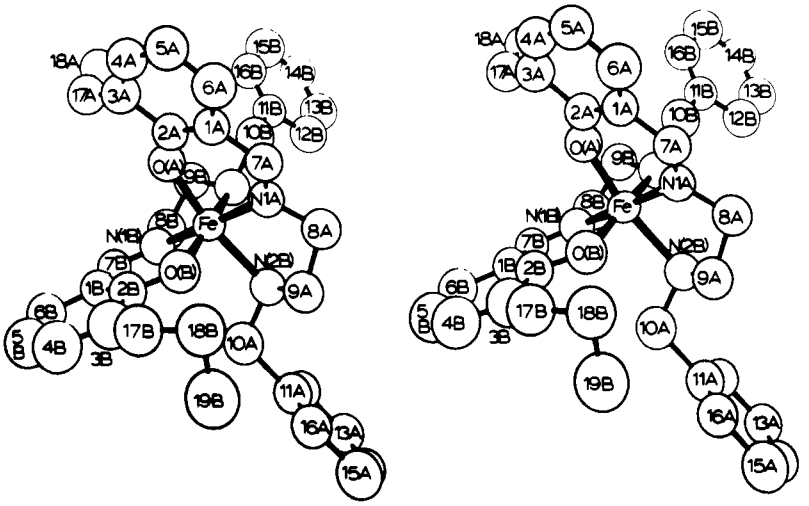

Figure 1. Stereoview of the $[Fe(3\text{-}AllSalBzen)_2]^+$ cation.

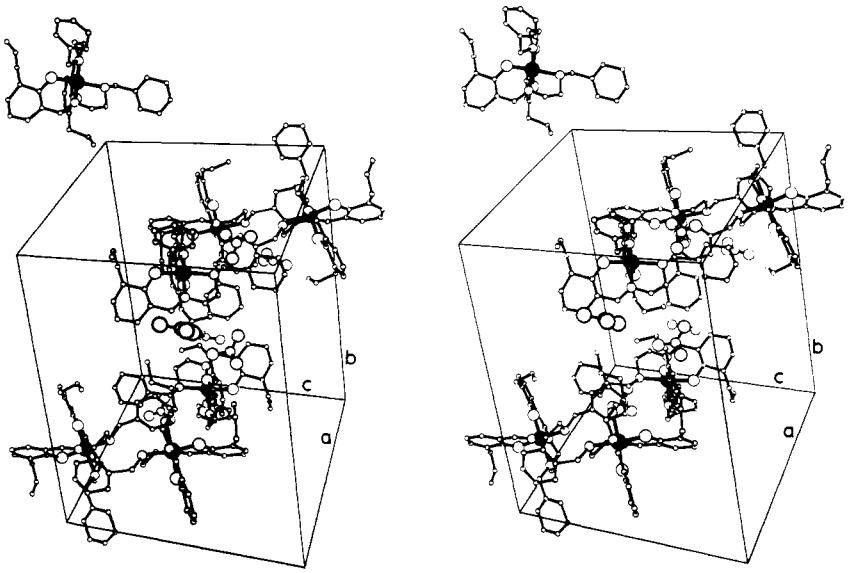

Figure 2. Stereoview of the molecular packing in the unit cell of $[Fe(3\text{-}All\text{-}SalBzen)_2]NO_3$.

Table III. Important Bond Lengths (Å) and Bond Angles (deg)

complex 1		complex 2	
	Bond Lengths		
Fe1–OA	1.941 (4)	Fe2–OC	1.864 (4)
Fe1–OB	1.852 (5)	Fe2–OD	1.903 (4)
Fe1–N1A	1.976 (5)	Fe2–N1C	1.949 (5)
Fe1–N2A	2.148 (5)	Fe2–N2C	2.031 (5)
Fe1–N1B	1.989 (5)	Fe2–N1D	1.924 (4)
Fe1–N2B	2.094 (5)	Fe2–N2D	2.063 (4)
	Bond Angles		
OA–Fe1–OB	94.36 (18)	OC–Fe2–OD	94.44 (16)
OA–Fe1–N1A	89.72 (18)	OC–Fe2–N1C	94.57 (18)
OA–Fe1–N2A	170.04 (18)	OC–Fe2–N2C	176.46 (17)
OA–Fe1–N1B	89.41 (19)	OC–Fe2–N1D	86.19 (17)
OA–Fe1–N2B	88.08 (19)	OC–Fe2–N2D	87.76 (16)
OB–Fe1–N1A	92.27 (20)	OD–Fe2–N1C	86.97 (18)
OB–Fe1–N2A	89.15 (19)	OD–Fe2–N2C	87.90 (17)
OB–Fe1–N1B	90.97 (21)	OD–Fe2–N1D	92.37 (17)
OB–Fe1–N2B	170.16 (21)	OD–Fe2–N2D	174.28 (16)
N1A–Fe1–N2A	80.82 (18)	N1C–Fe2–N2C	82.88 (19)
N1A–Fe1–N1B	176.70 (21)	N1C–Fe2–N1D	179.03 (20)
N1A–Fe1–N2B	97.29 (20)	N1C–Fe2–N2D	98.13 (17)
N2A–Fe1–N1B	99.89 (19)	N2C–Fe2–N1D	96.38 (19)
N2A–Fe1–N2B	90.03 (19)	N2C–Fe2–N2D	90.16 (17)
N1B–Fe1–N2B	79.51 (22)	N1D–Fe2–N2D	82.49 (17)

workers solved both room-temperature and low-temperature (103 K) structures and observed not only crystallographically independent sites with different spin-state fractions but also differences in the temperature-dependent transformations at the two sites.

Magnetic and Spectroscopic Characterization of $[Fe(3\text{-}All\text{-}SalBzen)_2]NO_3$. The partial spin-crossover nature of $[Fe(3\text{-}All\text{-}SalBzen)_2]NO_3$, inferred from the single-crystal structural work, agrees reasonably well with other physical characterizations of a microcrystalline sample of this material. Variable-temperature magnetic susceptibility data reveal a very gradual spin-crossover transition (3.02 μ_B at 286 K, 2.47 μ_B at 204 K, 2.01 μ_B at 103 K, 1.88 μ_B at 4.2 K; a complete data set is available[19]). The room-temperature magnetic moment is in agreement with the single-crystal X-ray structural results, where one of the cation sites is low spin and the other is a mixture of ca. 67% low spin/33% high spin. Assuming μ_{eff}(HS) to be 5.9 μ_B and μ_{eff}(LS) to be 1.88 μ_B, a population-weighted-average magnetic moment is calculated to be 2.95 μ_B, a number very similar to the experimental value at 286 K. Additionally, the room-temperature EPR spectrum (Figure 3) exhibits a weak absorption at $g \approx 4$, typical for high-spin ferric centers, and a strong axial signal ($g_\perp = 2.183$, $g_\parallel = 1.960$), typical for low-spin ferric centers of this type.[14] Although a Mössbauer spectrum obtained at 5 K revealed a low-spin ferric signal (CS = 0.09 (1) mm/s, QS = 2.62 (1) mm/s), data collection at elevated temperatures ($\gtrsim$100 K) was hampered by a low signal-to-noise ratio.

Spin-Crossover Transition in $[Fe(3\text{-}OEt\text{-}SalBzen)_2]BPh_4\cdot CH_3CN$. In order to investigate the solid-state spin-state lifetimes of these $Fe(N_4O_2)$ complexes, it was necessary to isolate a solid that undergoes a more complete spin-crossover transition than does

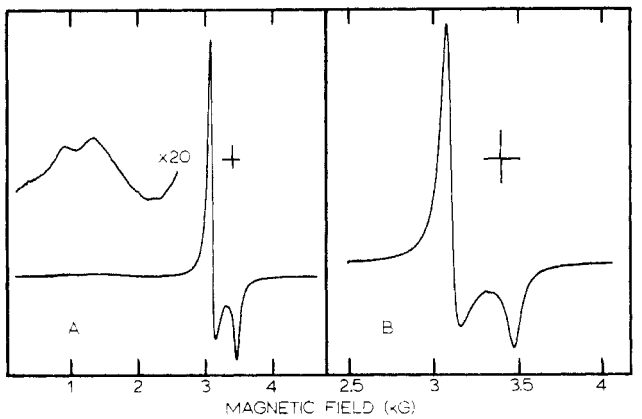

Figure 3. Room-temperature X-band EPR spectrum of [Fe(3-All-SalBzen)$_2$]NO_3.

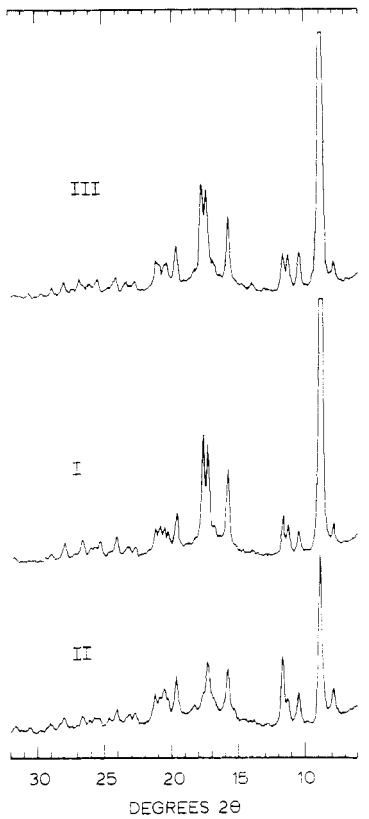

Figure 4. Room-temperature X-ray powder patterns of compounds I–III.

[Fe(3-All-SalBzen)$_2$]NO_3. After a number of permutations of salicylaldehyde substituents and counterions were screened, [Fe(3-OEt-SalBzen)$_2$]BPh_4·CH_3CN was found to show the most complete transformation (vide infra). This sample was examined in the three forms described in detail in the Experimental Section and summarized here: (I) [Fe(3-OEt-SalBzen)$_2$]BPh_4·CH_3CN (unperturbed); (II) [Fe(3-OEt-SalBzen)$_2$]BPh_4·CH_3CN (ground in mortar and pestle); (III) [Fe(3-OEt-SalBzen)$_2$]BPh_4 (solvate removed at 60 °C under vacuum). Illustrated in Figure 4 are room-temperature X-ray powder patterns of the three samples. The strong similarity of the three patterns makes it clear that, at most, only small structural changes accompany the perturbation in II and III.

Magnetic Susceptibility. Variable-temperature (300–20 K) magnetic susceptibility data for I–III are illustrated in Figure 5 and tabulated elsewhere.[19] The spin-crossover transformations are quite gradual but nearly complete. The high-spin fraction of I is, for example, 0.93 at 300 K and drops to 0.03 at 10 K. Also evident from Figure 5 is the influence of sample grinding on the spin-crossover transformation (I vs. II). The effect of sample grinding, i.e., a slight increase in the high-spin fraction at each

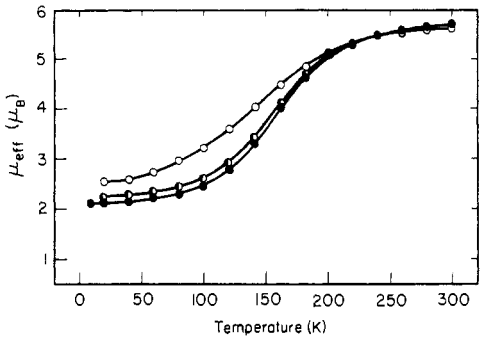

Figure 5. Plots of effective magnetic moment per iron ion, μ_{eff}/Fe, vs. temperature for the compounds I (●), II (◐), and III (○).

temperature, is similar to what has been seen for [Fe(Sal-Een)$_2$]PF_6[14] and for several Co(II) gradual spin-crossover systems.[23] Although the grinding phenomenon is not well understood, it has been suggested[14,24] that it may be the high-spin sites proximate to defects or the crystal surface that do not undergo the spin-state transformation at low temperature. It is also possible that grinding results in local heating of the sample and subsequent loss of a small percentage of the solvated acetonitrile. In any event, considering the relatively small impact that grinding has on the magnetic properties of I, it is not surprising that the spectroscopic characteristics of I and II are virtually identical. Consequently, we do not present any spectroscopic data for II in this report. Such data may be found elsewhere.[25]

The effect of desolvation (I vs. III) is also evident from Figure 5. This effect, more pronounced than sample grinding, also leads to a greater persistent high-spin fraction at low temperatures for III. That solvation (and desolvation) affects the spin-crossover transformation is well-known. Even noncoordinating solvents, such as methylene chloride and benzene, can dramatically influence the relative spin-state fractions. For example,[26] the dichloromethane-solvated ferric tris(morpholinecarbodithioate) complex is high spin, the benzene-solvated material is almost totally low-spin (μ_{eff} at 300 K is 2.92 μ_B), and the desolvated forms of both materials are gradual spin-crossover compounds. The effect of desolvation that we see for III is relatively small and is consistent with the apparently minor structural changes that accompany desolvation.

As was the case for the ferric X-SalEen and X-Salmeen complexes, the magnetic behavior of the complex cation [Fe(3-OEt-SalBzen)$_2$]$^+$ is strongly influenced by its counterion. The chloride and nitrate salts are essentially high-spin. The chloride salt exhibits a temperature-independent magnetic moment of 5.6 (1) μ_B from 280 K down to 8 K, and the temperature-independent moment of the nitrate salt is 5.1 (1) μ_B to 20 K.

Electron Paramagnetic Resonance. If distinct high- and low-spin EPR signals are present, variable-temperature EPR measurements provide a method for examining the microscopic environment about the ferric centers as the spin-crossover transformation develops. In addition, the observation of distinct spin-state signals indicates that the spin-state interconversion rates are slow relative to the X-band EPR time scale (ca. 10^{10} s^{-1}).

Low-spin ferric centers in pseudooctahedral ligand environments typically exhibit axial or rhombic resonances near $g = 2$. Following Griffith[27] (and, more recently, Bohan[28]), the experimental **g**-tensor components can be used to determine the d-orbital character of the lowest energy Kramers doublet of $^2T_{2g}$ origin. The combined effects of a low-symmetry crystal field and spin–orbit coupling split the $^2T_{2g}$ state into three Kramers doublets. In this work an analysis approach identical with that discussed by Haddad et al.[14]

(23) Müller, E. W.; Spiering, H.; Gütlich, P. *Inorg. Chem.* **1984**, *23*, 119.
(24) König, E.; Ritter, G.; Kulshreshtha, S. K. *Inorg. Chem.* **1984**, *23*, 1144.
(25) Timken, M. D. Ph.D. Thesis, University of Illinois, 1985.
(26) Malliaris, A.; Papaefthimiou, V. *Inorg. Chem.* **1982**, *21*, 770.
(27) Griffith, J. S. "The Theory of Transition Metal Ions"; Cambridge University Press: London, 1961; p 364.
(28) Bohan, T. L. *J. Magn. Reson.* **1977**, *26*, 109.

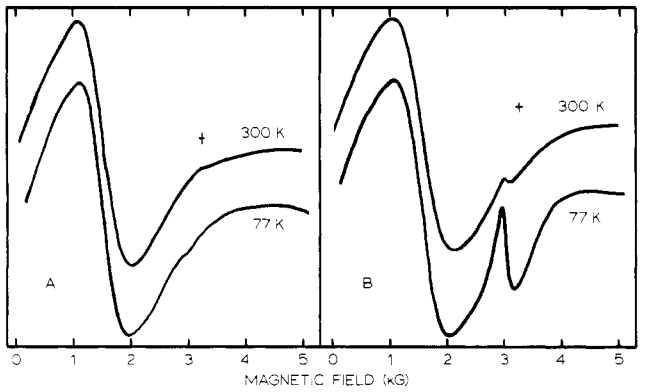

Figure 6. EPR spectra (X-band) of (A) $[Fe(3\text{-}OEt\text{-}SalBzen)_2]NO_3$ and (B) $[Fe(3\text{-}OEt\text{-}SalBzen)_2]Cl$.

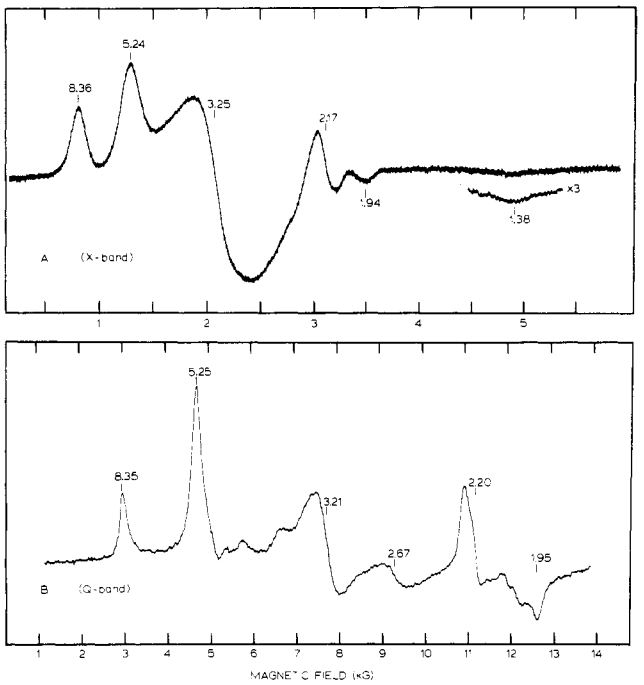

Figure 7. Room-temperature EPR spectra of I: (A) X-band; (B) Q-band. Effective g values are indicated.

was used to determine the d-orbital character and relative energy of each of these three Kramers doublets.

The *effective g* values for *high-spin* ferric systems are determined by the zero-field splitting (ZFS) of the ^6A electronic state. Wickman et al.[29] have used the Hamiltonian

$$\mathcal{H} = D(S_z^2 - \tfrac{1}{3}S(S+1)) + E(S_x^2 - S_y^2) + gH\cdot S$$

to describe the combined effects of axial ZFS (D), rhombic ZFS (E), and the Zeeman interaction (with $g = 2.0$) on the ^6A electronic term. The *effective g* values (g^e) that result from this analysis depend primarily on the ratio E/D. At the rhombic extreme ($E/D = 1/3$) an isotropic $g^e \simeq 4.3$ is expected; at the axial extreme ($E/D \simeq 0$) effective g values of 2 and 6 are predicted. Both of these circumstances are common in the literature for high-spin ferric complexes. Although cases of intermediate rhombicity ($0.1 < E/D < 0.2$) have been reported,[30] they are less frequently encountered.

We should point out that the effective g values were calculated by assuming the axial ZFS splitting parameter D to be greater than the Zeeman term (0.3 cm^{-1} for X-band fields, 1 cm^{-1} for Q-band fields). Although we have no precise knowledge of the ZFS values for the complexes reported here, this assumption is apparently quite good (vide infra).

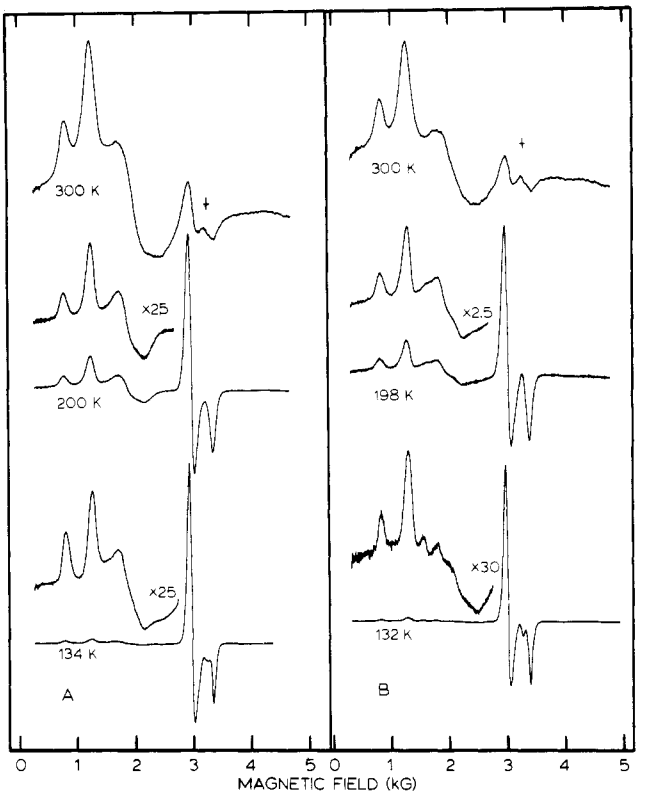

Figure 8. Variable-temperature X-band EPR spectra for I (A) and III (B).

Figure 6 illustrates EPR spectra for the basically high-spin chloride and nitrate salts of $[Fe(3\text{-}OEt\text{-}SalBzen)_2]^+$. At room temperature, both samples exhibit broad $g^e \simeq 4.1$ signals typical for the high-spin rhombic case. The $g \simeq 2$ signal evident at 77 K for the nitrate salt is due to the presence of low-spin ferric molecules.

In contrast, the spectra illustrated in Figure 7 for the BPh_4^- salt I are quite complex and exhibit X-band absorption from 800 to 5000 G. Because the magnetic susceptibility results indicate that I is 93% high spin at room temperature, we assign the axial signal near $g = 2$ ($g_\parallel \simeq 1.94$, $g_\perp \simeq 2.2$) to the 7% low-spin population. The remaining signals are due to the high-spin species. These signals can be understood in terms of Wickman's analysis. With the use of the eigenfunctions and expressions provided in ref 29, the following three effective **g** tensors were calculated for the three Kramers doublets with $E/D = 0.15$: $\mathbf{g}_1^e = (2.71, 8.68, 1.44)$, $\mathbf{g}_2^e = (3.13, 2.82, 5.38)$, $\mathbf{g}_3^e = (0.16, 0.14, 9.95)$. These values are in good agreement with the experimentally observed effective g values: $\mathbf{g}_1^e = (2.67, 8.35, 1.38)$, $\mathbf{g}_2^e = (3.25, -, 5.24)$, $\mathbf{g}_3^e = (-, -, -)$. That four of the predicted g values went undetected is not surprising. The $g^e = 2.82$ signal probably overlaps strongly with the $g^e = 3.2$ signal, and the three $\mathbf{g}_3^e$ resonances occur at very low and very high fields. It is also evident from Figure 7 that the X- and Q-band spectral patterns are quite similar, from which it can be inferred that $D >> g\beta H \simeq 1$ cm^{-1}.

The expected sensitivity of the high-spin ferric EPR resonances to E/D provided motivation for a more detailed examination of the EPR properties of I and III. That E/D for the cation $[Fe(3\text{-}OEt\text{-}SalBzen)_2]^+$ is sensitive to solid-state perturbations is evident by comparing Figures 6 and 7. This apparent sensitivity suggested that the high-spin EPR signals should be an excellent probe for subtle distortions of the high-spin site through the course of the thermal spin-crossover transition. Representative spectra, as a function of temperature, for I and III are illustrated in Figure 8. The spin-crossover nature of both samples is evident; the low-spin axial **g** tensor ($g_\parallel = 2.18$, $g_\perp = 1.94$) increases in intensity

(29) Wickman, H. H.; Klein, M. P.; Shirley, D. A. *J. Chem. Phys.* **1965**, *42*, 2115.

(30) (a) McCann, S. W.; Wells, F. V.; Wickman, H. H.; Sorrell, T. N.; Collman, J. P. *Inorg. Chem.* **1980**, *19*, 621. (b) Peisach, J.; Blumberg, W. E. *Proc. Natl. Acad. Sci. U.S.A.* **1970**, *67*, 172. (c) Friedrich, M.; Karthe, W. *Phys. Status Solidi B* **1977**, *80*, K127.

Table IV. Experimental[a] and Calculated EPR Parameters

	[Fe(3-All-SalBzen)$_2$]NO$_3$	I	III
g_x	−2.183	−2.183	−2.194
g_y	2.183	2.183	2.194
g_z	−1.960	−1.936	−1.955
k	0.832	0.673	0.836
A_1[b]	−0.049	0.064	−0.052
B_1[b]	−0.999	0.998	−0.999
C_1[b]	0.000	0.000	0.000
E_1/λ[c]	−9.89	−7.66	−9.34
E_2/λ[c]	4.43	3.31	4.15
E_3/λ[c]	4.46	3.35	4.19

[a] Experimental data (X-band) on microcrystalline samples at 77 K. [b] The orbital coefficients for the wave function describing the lowest electronic state of $^2T_{2g}$ origin: $\psi = A|+1^+\rangle + B|\zeta^-\rangle + C|-1^+\rangle$. [c] The relative energies of the three orbital states of $^2T_{2g}$ origin.

at low temperatures at the expense of the high-spin signals. Although the high-spin signal *intensity* is strongly temperature dependent, a close inspection of these spectra reveals no detectable temperature dependence of the effective g values. Particularly, note that the well-defined low-field signals (g^e = 8.36, 5.25) exhibit changes only in intensity; *no shifts of the resonance fields* with temperature are evident. From these observations we infer that the ratio E/D remains constant throughout the spin-crossover transformation.

This constancy of E/D is somewhat surprising in light of the relatively large intramolecular distortions (i.e., Fe–L distances, vide supra) that accompany spin-state interconversions. If the gradual spin-crossover transformation in this solid occurs via the random, solid-solution mechanism suggested by König,[5] then at intermediate temperatures high-spin molecular ions should experience a variety of solid-state environments. For example, a high-spin ferric center could be surrounded entirely by low-spin nearest neighbors at one extreme and surrounded entirely by high-spin molecules at the other extreme. It might be anticipated that a range of ZFS values, a range of E/D ratios, and a range of high-spin EPR signals would be seen. On the other hand, it is possible that the neighbor–neighbor interactions in these BPh_4^- lattices are too weak to influence E/D. In this case, we would expect little or no change in the high-spin EPR signal as the spin-crossover transformation proceeds. It is interesting that the high-spin effective g values for I and III are identical, an observation that gives some credence to the argument that intermolecular interactions may play an insignificant role in determining E/D in these BPh_4^- solids.

The temperature-independent E/D ratio is also consistent with a domain mechanism[1] for the spin-crossover transition. In this case, the high-spin molecular ions would always be in a totally high-spin domain with only high-spin neighbors. Temperature-independent high-spin ZFS parameters would be expected. We do not, however, have any further evidence for (or against) the existence of domains in these solids. A third possibility, that D and E change significantly with temperature but the ratio of E/D remains constant, is considered to be unlikely.

The low-spin axial g values of I were analyzed as previously described,[14] and the results are listed in Table IV. The values in this table are consistent with the results for most other ferric N_4O_2 low-spin molecules.[12,14] That is, the eigenfunction of the lowest energy Kramers doublet of $^2T_{2g}$ origin is essentially a d_{xy} hole. This result is in agreement with Mössbauer data for this compound (vide infra). Furthermore, the g-value analysis indicates that the first excited Kramers doublet is roughly 5000 cm^{-1} higher in energy than the ground-state Kramers doublet (assuming λ-(Fe^{III}) = 460 cm^{-1}). This energy separation, much larger than thermal energies, indicates that both the low-spin magnetic moment and Mössbauer quadrupole splitting should be essentially temperature independent up to 300 K. The low-spin EPR g values of I and II are identical within experimental error. Table IV also gives experimental g values, orbital coefficients, and relative electronic state energies for III and [Fe(3-All-SalBzen)$_2$]NO$_3$.

Mössbauer Spectroscopy. The Mössbauer effect has proven to be an important tool for the study of iron spin-crossover solids in that it can provide information about the relative amounts of high- and low-spin species, the microscopic environments of the ^{57}Fe nuclei, and the spin-state interconversion rates. Figure 9 illustrates variable-temperature Mössbauer spectroscopic data for the ^{57}Fe-enriched compounds for I and III. The solid lines for each spectrum represent a computer fitting to Lorentzian line shapes; least-squares fitting parameters are provided in Tables V and VI.[19] As will be discussed later, the numbers obtained from these fittings must be considered with caution because of the intrinsic non-Lorentzian nature of the Mössbauer absorptions.

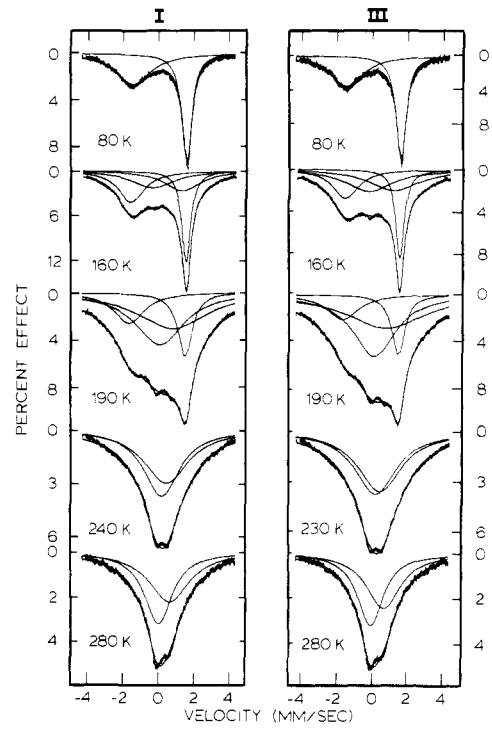

Figure 9. Variable-temperature ^{57}Fe Mössbauer spectra of I (left side) and III (right side). The solid lines represent computer fittings of the absorptions to Lorentzian line shapes.

Both I and III exhibit a strongly asymmetric low-spin quadrupole doublet at 80 K (I, CS = 0.36 (1) mm/s, QS = 2.90 (1) mm/s, $\Gamma_{1/2}(-)$ = 1.15 (2) mm/s, $\Gamma_{1/2}(+)$ = 0.33 (1) mm/s; III, CS = 0.34 (1) mm/s, QS = 2.93 (1) mm/s, $\Gamma_{1/2}(-)$ = 1.11 (2) mm/s, $\Gamma_{1/2}(+)$ = 0.33 (1) mm/s). Such line width asymmetry is not atypical for well-isolated low-spin ferric molecules[12,14,31] and is the result of relatively long paramagnetic relaxation times for these molecules. More precisely, the spin–lattice and spin–spin relaxation times are comparable to the ^{57}Fe nuclear Larmor precession time. As a result, the internal magnetic field experienced by the ^{57}Fe nucleus is not averaged to zero over the lifetime of the nuclear excited state, and the Zeeman splitting of the nuclear M_I levels broadens the Mössbauer transitions ($|I_g,M_{Ig}\rangle \rightarrow |I_e,M_{Ie}\rangle$). As discussed by Blume,[32] the $|^1/_2,\pm^1/_2\rangle \rightarrow |^3/_2,\pm^3/_2\rangle$ transitions are broadened more than are the $|^1/_2,\pm^1/_2\rangle \rightarrow |^3/_2,\pm^1/_2\rangle$ transitions. For both I and III the broad negative velocity quadrupolar component corresponds to the $|^1/_2,\pm^1/_2\rangle \rightarrow |^3/_2,\pm^3/_2\rangle$ transition. Consequently, V_{zz} (the principal axis component of the electric field gradient tensor) is negative, a conclusion consistent with the d_{xy} ground state inferred from EPR g-tensor analyses. Similar observations have been made for the related [Fe(X-Sal-Een)$_2$]$^+$ complexes.[14]

It is likely that spin–lattice relaxation times are long due to the large energy separation of the ground and first-excited spin-doublet electronic states. Spin–spin relaxation times are attenuated

(31) Wickman, H. H.; Trozzolo, A. M. *Phys. Rev. Lett.* **1965**, *15*, 156.
(32) Blume, M. *Phys. Rev. Lett.* **1965**, *14*, 96.

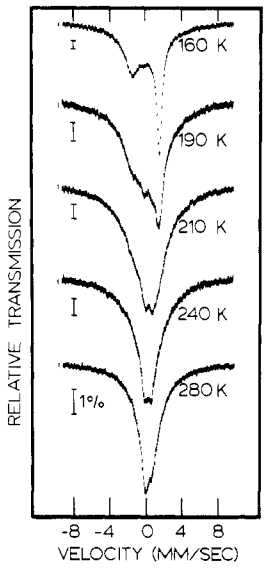

Figure 10. Variable-temperature ^{57}Fe Mössbauer spectra of I.

by the long Fe–Fe distances arising from the isolation provided by the large BPh_4^- counterions.

It is evident from Figure 9 that marked spectral changes accompany the spin-crossover transformations for I and III. As the temperatures of the sample is increased, a very broad high-spin quadrupole-split doublet increases in intensity. Up to at least 190 K the high- and low-spin signals are distinct, and we can infer that the spin-state interconversion rates are slow relative to the Mössbauer time scale. Above 210 K it is not possible to distinguish signals for the high- and low-spin species, even though magnetic susceptibility studies indicate that an appreciable low-spin population is present at these temperatures. However, due to the extreme line widths of the high-spin absorptions and the decreasing relative intensities of the low-spin components, we cannot definitively conclude that the spin-state interconversion rates become faster than the Mössbauer time scale. Such a conclusion is only a possibility.

Figure 10 further illustrates the extremely broad line widths of the high-spin signals; absorption intensity is evident out to nearly ±10 mm/s. As was the case for the low-spin molecules, slow paramagnetic relaxation is likely the major origin of the broad line widths. The paramagnetic relaxation rates for I and III are not sufficiently slow relative to the ^{57}Fe nuclear Larmor precession frequency to result in the six-line patterns typically seen for slowly relaxing high-spin ferric centers. Instead, the relaxation rates are *intermediate*, *i.e.*, on the order of the nuclear Larmor precession frequency. Consequently, the Mössbauer absorptions are intrinsically non-Lorentzian and our computer fittings of the data to four (and two) Lorentzian line shapes must be viewed with caution. As well as making the parameters listed in Tables V[19] and VI[19] highly uncertain, the extreme line widths lead to a general overestimation of the high-spin absorption fraction.

A quantitative analysis of this intermediate relaxation data would require, in principle, the use of a time-dependent Hamiltonian such as described by Wickman[33] or Blume.[34] We have not attempted such an analysis due to the practical complexities of combining the intermediate paramagnetic relaxation with the spin-crossover transition. In an attempt to alleviate this problem, Mössbauer spectra were run for the ^{57}Fe-enriched sample of $[Fe(3\text{-}OEt\text{-}SalBzen)_2]BPh_4\cdot CH_3CN$ in an external magnetic field of 60 kG. External field (60 kG) spectra were run at both 280 and 240 K. Unfortunately, at both temperatures the spectra look very similar to those shown in Figure 10. Only small changes in line shape could be seen.

Conclusions

The spin-crossover transformations in these N_4O_2 ferric complexes have been examined structurally, magnetically, and spectroscopically. The room-temperature X-ray structure of $[Fe(3\text{-}All\text{-}SalBzen)_2]NO_3$ shows two crystallographically independent cations, one low spin and the other part high spin and part low spin. It is quite possible that many of the "incomplete" spin-crossover transformations that have been reported are actually such "two-site" transitions, where one site undergoes a relatively complete transformation and the other remains either totally high or low spin.

The cation $[Fe(3\text{-}OEt\text{-}SalBzen)_2]^+$ is essentially high spin in its Cl^- and NO_3^- salts, but it behaves as a spin-crossover complex in the BPh_4^- salt. Variable-temperature spectroscopic examinations of $[Fe(3\text{-}OEt\text{-}SalBzen)_2]BPh_4\cdot CH_3CN$ indicate spin-state interconversion rates less than 10^{10} s^{-1} up to 300 K and less than 10^7 s^{-1} up to 190 K. Variable-temperature EPR studies show a surprisingly constant high-spin ferric E/D ratio, a result that can be rationalized in terms of either the solid–solution spin-crossover mechanism or the domain mechanism. Slow paramagnetic relaxation for both the high- and low-spin electronic states results in sharp, well-resolved EPR signals, but extremely broad Mössbauer absorptions. Consequently, we have been unable to characterize conclusively the spin-state interconversion rate above 190 K.

Acknowledgment. We are grateful for support from the National Institutes of Health, Grant HL13652 (D.N.H.).

Registry No. $[Fe(3\text{-}OEt\text{-}SalBzen)_2]NO_3$, 98652-17-6; $[Fe(3\text{-}OEt\text{-}SalBzen)_2]Cl$, 98652-18-7; $[Fe(3\text{-}OEt\text{-}SalBzen)_2]BPh_4$, 98652-21-2; $[Fe(3\text{-}OEt\text{-}SalBzen)_2]BPh_4\cdot CH_3CN$, 98652-22-3; $[Fe(3\text{-}All\text{-}SalBzen)_2]NO_3$, 98652-20-1; ^{57}Fe, 14762-69-7; *N*-benzylethylenediamine, 4152-09-4; 3-ethoxysalicylaldehyde, 492-88-6; 3-allylsalicylaldehyde, 24019-66-7.

Supplementary Material Available: Tables V and VI (Mössbauer least-squares fitting parameters), Table VII (thermal parameters), Tables VIII–XIII (magnetic susceptibility data), and a table of observed and calculated structure factors (31 pages). Ordering information is given on any current masthead page.

(33) Wickman, H. H.; Klein, M. P.; Shirley, D. A. *Phys. Rev.* **1966**, *152*, 345.
(34) Blume, M.; Tjon, J. A. *Phys. Rev.* **1968**, *165*, 446.